

# In Situ X-ray Scattering Study of the Passive Film on Ni(111) in Sulfuric Acid Solution

O. M. Magnussen,<sup>\*,†</sup> J. Scherer,<sup>†</sup> B. M. Ocko,<sup>‡</sup> and R. J. Behm<sup>†</sup>

*Abteilung Oberflächenchemie und Katalyse, Universität Ulm, D-89069 Ulm, Germany, and  
Physics Department, Brookhaven National Laboratory, Upton, New York 11973*

*Received: October 11, 1999*

Results of an in situ X-ray scattering study of the passive film formed on Ni(111) electrodes by passivation in 0.05 M H<sub>2</sub>SO<sub>4</sub> (pH 1.0) at 0.50 V<sub>Ag/AgCl</sub> are reported and compared with results on the film formed by oxidation in air at room temperature. In both cases, ultrathin, (111)-oriented NiO films are observed, which are aligned with the Ni substrate lattice and slightly expanded along the surface normal with respect to bulk NiO. However, two major structural differences are found: (i) while on the air-formed oxide parallel (NiO-[110] || Ni[110]) and antiparallel (NiO[110] || Ni[110]) oriented domains coexist, the passive film exhibits a well-defined antiparallel orientation and (ii) the lattice of the passive film is, in contrast to that of the air-formed oxide, tilted relative to the substrate with a broad angular dispersion of the tilt angle centered at about 3.3°.

## 1. Introduction

The surfaces of almost all metals, including the technologically important transition metals Cr, Fe, and Ni, are protected in aqueous electrolytes or moist air by ultrathin oxide/hydroxide films, which stabilize these reactive metals against corrosion. The atomic and defect structure of these passive films is of fundamental importance for the corrosion behavior of these metals and accordingly has been studied extensively.<sup>1,2</sup> In the past, these studies were limited to electrodes emersed from the electrolyte and transferred into UHV (ex situ studies). It is not clear, however, if and how the transfer into UHV affects the structure of the passive film in these studies. Only recently were in situ studies of the structure of passive films in liquid environment by scanning probe microscopy (STM, AFM), X-ray spectroscopy (XANES, EXAFS), and surface X-ray scattering (SXS) reported. In particular, the latter technique can provide detailed information on the (three-dimensional) crystal structure, lattice parameters, and defects, as demonstrated for passive films on Ti<sup>3</sup> and Fe.<sup>4,5</sup> Here we present the first in situ SXS study of passive films formed on a Ni surface.

Previous studies have shown that passivated Ni electrodes are covered by a dense oxide film, which is responsible for the excellent corrosion resistance of nickel.<sup>1,2</sup> With various methods and under different experimental conditions, it was found that passive films in sulfuric acid are a few atomic layers thick and composed of NiO and Ni(OH)<sub>2</sub>.<sup>6–8</sup> In these studies a duplex structure was proposed, consisting of an inner layer of crystalline NiO and an outer film of amorphous Ni(OH)<sub>2</sub>. Ex situ RHEED studies showed that the crystalline part of the passive film on Ni(111) formed in sulfuric acid solutions consists of nearly stoichiometric NiO(111).<sup>9–11</sup> Atomic resolution STM observations of the passive film on Ni(111) were first reported by Maurice et al.,<sup>12,13</sup> who studied the surface structure of passivated electrodes ex situ in air. They observed a hexagonal atomic lattice with a lattice constant close to bulk NiO and a characteristic step structure, which was attributed to an oxide

phase tilted with respect to the Ni substrate lattice. These results were later confirmed by in situ STM studies of Suzuki et al.<sup>14</sup> and Zuili et al.<sup>8</sup> A fundamental limitation of these studies is, however, that lattice distances can be measured by STM only at the surface and with relatively low precision. Hence, as the lattice parameters of different Ni oxide/hydroxide phases are rather similar, an unambiguous determination of the passive film structure was not possible. Furthermore, due to the local character of the STM measurements, quantitative data on the surface morphology, such as average grain sizes, can only be obtained by elaborate statistical analysis, which has not been performed up to now.

In the present study, the limitations associated with ex situ and STM measurements were overcome by investigating the oxide films on Ni(111) by X-ray diffraction, which allows a precise in situ determination of the (three-dimensional) lattice structure, including the internal film structure. As will be shown in the following, the oxide film formed by passivation of an atomically smooth, metallic Ni(111) surface in 0.05 M H<sub>2</sub>SO<sub>4</sub> is composed of small crystallites of (111)-oriented, slightly distorted NiO. The structure of the film will be discussed in detail and compared to that of the oxide film formed in air at room temperature and to bulk NiO. It will be shown that the passive film structure differs distinctly from the structure of air-formed oxides and emersed passive films. This demonstrates the importance of in situ studies and has important consequences for the corrosion behavior of Ni.

## 2. Experimental Section

The experiments were performed at beamline X22A of the National Synchrotron Light Source with a similar experimental setup as described in ref 15. Two Ni(111) single crystals (Mateck, 99.99%) were used, which were mechanically polished down to 0.03 μm and electropolished in ~57% H<sub>2</sub>SO<sub>4</sub>. The miscut of the samples was within 0.3°. Prior to each experiment, the sample was annealed for 3–15 h in a H<sub>2</sub> stream at 1273 K, cooled to room temperature, exposed to air, and then mounted in the sample holder. For the in situ experiments, the Ni crystal was immersed under potential control at potentials between

<sup>†</sup> Universität Ulm.

<sup>‡</sup> Brookhaven National Laboratory.

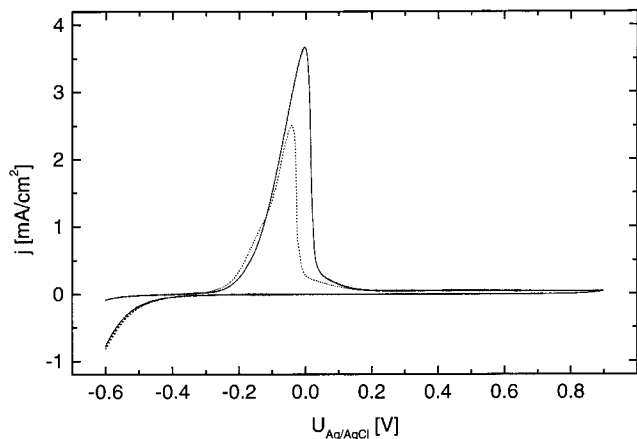


**Figure 1.** Cyclic voltammogram of a freshly annealed Ni(111) single crystal in 0.05 M  $\text{H}_2\text{SO}_4$  solution after 15 min reduction at  $-0.60$  V (scan rate 10 mV/s). The solid line shows the first scan after the reduction, the dotted line the stable voltammogram achieved after five potential cycles.

$-0.60$  and  $0.50$  V versus the Ag/AgCl (sat.) reference electrode in a cell for in situ SXS experiments similar to that in ref 15. All potentials are quoted with respect to this reference. X-ray diffraction data were recorded with the sample covered by a  $\sim 10$   $\mu\text{m}$  layer of electrolyte, which was contained by a  $4$   $\mu\text{m}$  prolene window and the cell surrounded by an  $\text{N}_2$  atmosphere for deoxygenation of the electrolyte. During electrochemical reduction or passivation, the prolene window was inflated. The ex situ experiments were performed under  $\text{N}_2$  in the same cell. The X-ray data were obtained at a wavelength of  $1.20$   $\text{\AA}$  using a liquid  $\text{N}_2$ -cooled Ge detector to suppress the inelastic background caused by fluorescence from the bulk Ni crystal. Resolution was limited by  $2$  mm slits corresponding to an detector acceptance of  $3$  mrad or by  $1$  mrad Soller slits and by the mosaic spread of the Ni single crystals of  $0.04$ – $0.10^\circ$ . The hexagonal coordinate system<sup>15</sup> of the Ni(111) substrate was used, where  $Q = (a_{\text{Ni}}^*, b_{\text{Ni}}^*, c_{\text{Ni}}^*) \cdot (H, K, L)$  with the lattice vectors  $a_{\text{Ni}}^* = b_{\text{Ni}}^* = 8\pi/\sqrt{6}a = 2.912$   $\text{\AA}^{-1}$  parallel and  $c_{\text{Ni}}^* = 2\pi/\sqrt{3}a_{\text{Ni}} = 1.029$   $\text{\AA}^{-1}$  perpendicular to the Ni surface ( $a_{\text{Ni}} = 3.5238$   $\text{\AA}$ ). The crystallographic data were obtained from four and six independent experiments on the air-formed and the passive film, respectively.

### 3. Results and Discussion

A typical cyclic voltammogram of Ni(111) in  $0.05$  M  $\text{H}_2\text{SO}_4$  (pH 1.0), recorded in a separate electrochemical cell in hanging meniscus geometry, is shown in Figure 1. The crystal was prepared using the same method as in the X-ray measurements. After immersion under potential control at  $-0.60$  V, the sample was kept for 15 min at this potential in order to electrochemically reduce the air-formed oxide. In the subsequent anodic potential sweep (solid line), the characteristic passivation behavior with a single irreversible peak at  $0.00$  V, indicating Ni dissolution and passive film formation, is observed. This agrees well with previous results of  $\text{H}_2$ -annealed Ni(111) electrodes in sulfuric acid solutions.<sup>8,14</sup> In subsequent potential cycles, peak position and height shift slightly until a stable voltammogram is obtained (dashed line). Similar voltammograms but with contributions of the (polycrystalline) sample edges were obtained in the cell for the SXS experiments.

Prior to studies of the passive film, the air-formed oxide present on the surface after the annealing procedure was characterized by SXS. In these experiments, the diffraction

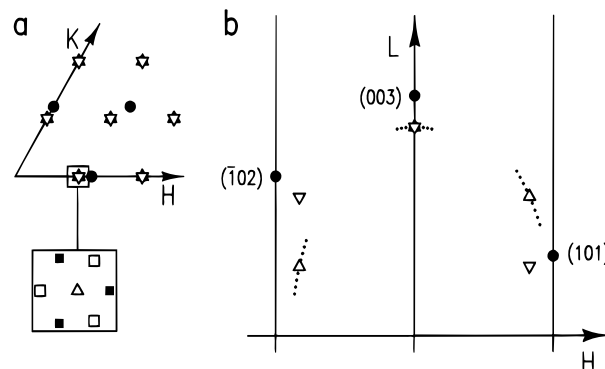


**Figure 2.** Reciprocal space pattern showing (a) the in-plane and (b) surface-normal positions of the Ni substrate peaks ( $\bullet$ ) and crystal truncation rods (solid lines) and of the NiO peaks with parallel ( $\nabla$ ) and antiparallel ( $\Delta$ ) orientation ( $\star$  indicates that the peak positions of both orientations overlap in the projection plane). The peak positions expected for oxide lattices tilted by an angle  $\alpha$  with respect to the substrate lattice are indicated as dots in (b) for  $\alpha = \pm 2, \pm 4, \pm 6,$  and  $\pm 8^\circ$  and in the inset in (a) for  $\alpha = +8^\circ$  (open squares) and  $\alpha = -8^\circ$  (closed squares) at the position of the  $(a_{\text{NiO}}^*, 0, 2c_{\text{NiO}}^*)$  peak (untilted phase denoted by  $\Delta$ ).

pattern (shown in Figure 2) exhibits broad peaks at  $(a_{\text{NiO}}^* \cdot h', a_{\text{NiO}}^* \cdot k', c_{\text{NiO}}^* \cdot (h' + 2k' + 3l'))$  and at  $(a_{\text{NiO}}^* \cdot h', a_{\text{NiO}}^* \cdot k', c_{\text{NiO}}^* \cdot (2h' + k' + 3l'))$  where  $h', k', l' = 0, \pm 1, \pm 2, \dots$ . The reciprocal lattice spacings (in hexagonal Ni coordinates) are  $a_{\text{NiO}}^* = (0.834 \pm 0.001)a_{\text{Ni}}^*$  and  $c_{\text{NiO}}^* = (0.824 \pm 0.008)c_{\text{Ni}}^*$ , which give in-plane and surface normal lattice spacings of  $a_{\text{NiO}} = 2.988 \pm 0.004$   $\text{\AA}$  and  $c_{\text{NiO}} = 7.41 \pm 0.01$   $\text{\AA}$ . This diffraction pattern corresponds to two twin-related, (111)-oriented NiO phases with the in-plane orientation parallel ( $\text{NiO}[1\bar{1}0] \parallel \text{Ni}[1\bar{1}0]$ ) and antiparallel ( $\text{NiO}[1\bar{1}0] \parallel \text{Ni}[\bar{1}10]$ ) to the underlying Ni substrate lattice, i.e., the ABC Ni stacking sequence is followed by ABC or BAC NiO stacking, respectively. This is in agreement with previous electron diffraction data on the gas-phase oxidation of Ni(111),<sup>16–18</sup> which found both orientations in films of similar thickness as well as in thicker thermal oxide films, with the ratio depending on the sample preparation. Scans through the three low-order peaks (circles) are displayed in Figure 3. Scans along the surface normal direction (Figure 3a–c) exhibit very broad, overlapping peaks, reflecting the small thickness of the oxide layer, which is according to parallel X-ray reflectivity measurements  $7.2$ – $10.3$   $\text{\AA}$ .<sup>19</sup> For the radial (Figure 3d–f) and transverse scans (not shown) within the  $(H, K)$  plane, the peaks are well described by Gaussian peak shapes (solid lines in Figure 3d–f) with widths that are significantly broader than the spectrometer resolution (see below).

In the next stage of the experiments, the stability of the air-formed oxide on Ni samples immersed in  $0.05$  M  $\text{H}_2\text{SO}_4$  solution was characterized in situ in the X-ray electrochemical cell. Directly after immersion in the electrolyte at potentials between  $-0.40$  and  $-0.25$  V, the diffraction pattern is unaltered. At potentials  $\leq -0.40$  V, the air-formed oxide is gradually removed with the reduction rate rapidly increasing with decreasing potential. For example, small amounts of the oxide are found even after 1.5 h at  $-0.40$  V, whereas typically after 15 min reduction at  $-0.60$  V no diffraction peaks characteristic of NiO are detected. The removal of the oxide film and the low surface roughness of the resulting Ni electrode surface was demonstrated also in parallel measurements of the specular X-ray reflectivity and separate in situ STM experiments performed in an analogous way, which will be described elsewhere.<sup>19</sup>

After complete reduction of the air-formed oxide at  $-0.60$  V, the passive film was formed by an anodic potential step to

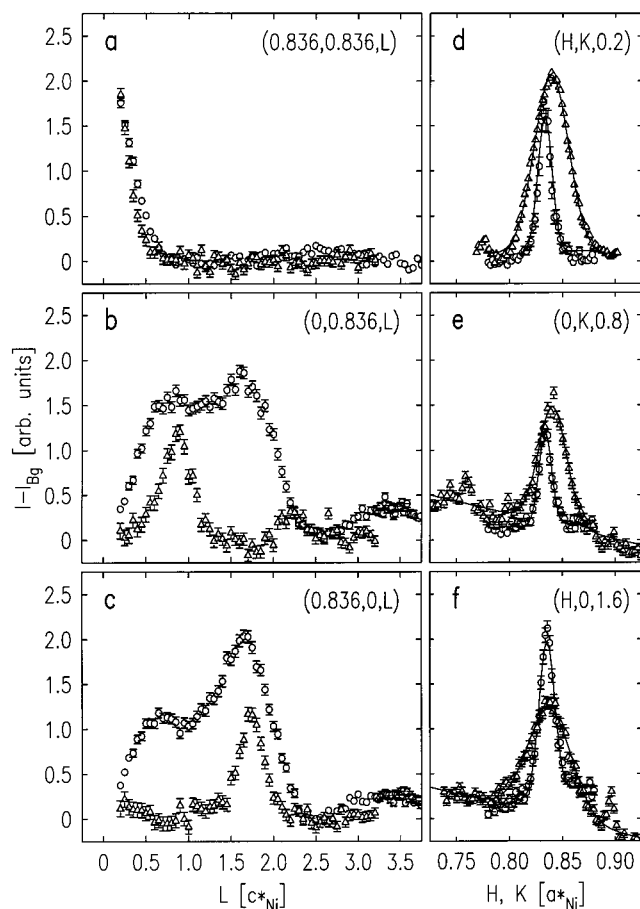


**Figure 3.** Peak profiles along (a–c)  $L$  and (d–f)  $q_L$  at the three low-order peak positions for the air-formed oxide in  $N_2$  (circles) and the passive film in 0.05 M  $H_2SO_4$  solution at 0.50 V (triangles). For the in situ data, the background scattering by the electrolyte and prolene window (obtained at  $\pm 7^\circ$ ) was subtracted. Gaussian fits to the peaks (see text) are shown as solid lines.

0.50 V. As indicated by the reflectivity and by in situ STM measurements, the passivation is accompanied by a significant increase in the surface roughness, probably due to Ni dissolution. The scans shown in Figure 3 (triangles) demonstrate that a similar (111)-oriented NiO layer as for oxidation in air is formed. A diffraction pattern characteristic for a (crystalline)  $Ni(OH)_2$  phase was not observed, in accordance with previous studies where the outer  $Ni(OH)_2$  layer was suggested to be amorphous.<sup>8</sup> In contrast to the air-formed oxide, only the peaks at  $(a_{NiO}^* \cdot h', a_{NiO}^* \cdot k', c_{NiO}^* \cdot (2h' + k' + 3l'))$ , corresponding to the antiparallel orientation, are found for the NiO formed by passivation, whereas the parallel-oriented NiO phase is apparently absent. Very similar results were obtained for passive films formed at other potentials.<sup>19</sup>

In addition, a film consisting exclusively of the antiparallel oriented NiO phase was also found on Ni samples immersed directly at 0.50 V without prior reduction of the air-formed oxide. Hence, the oxide structure can apparently be reverted to the preferred antiparallel orientation in the passive layer potential regime. This is supported by previous ex situ studies, where a higher tendency toward antiparallel orientation was observed on electropolished than on  $H_2$ -annealed samples after air exposure.<sup>18</sup> While direct conversion of the parallel to the antiparallel orientation would prove that the latter is more stable under electrochemical conditions, the real situation is more complex in that the oxide is continuously dissolved and reformed at the electrochemical interface.<sup>20,21</sup> In this situation, we cannot

distinguish whether the antiparallel phase is favored by energetic or kinetic effects. Finally, in ex situ SXS studies of passivated Ni electrodes, performed directly after in situ experiments on samples which were emersed from the electrolyte, rinsed with ultrapure water, and dried in a  $N_2$  stream, again similar peak intensities were found for the parallel and the antiparallel orientation. Hence, in this case, both orientations coexist with similar probability. This rather surprising behavior may be caused by a (partial) chemical NiO dissolution during the transfer procedure and subsequent NiO reformation or by conversion of the  $Ni(OH)_2$  component of the passive film due to dehydration. The peak widths along  $L$  for the emersed sample are identical to those obtained in situ for the passive film, indicating that the thickness of the crystalline part of the film does not change during the emersion (see below). According to these results, the oxide structure is directly affected by the environment, which demonstrates the importance of in situ measurements.

For the air-formed oxide, the Gaussian widths of the peaks within the surface plane, i.e., the radial and transverse widths  $\sigma_r$  and  $\sigma_t$ , are in good agreement with the above model of a perfectly (anti-)parallel lattice orientation with respect to the Ni substrate. Here, the same  $\sigma_r$  is found for all peaks corresponding to the same orientation (independent of their  $L$ -position), however, up to 90% larger widths for antiparallel ( $\langle \sigma_r \rangle = 0.034 \text{ \AA}^{-1}$ ) than for parallel orientation ( $\langle \sigma_r \rangle = 0.020 \text{ \AA}^{-1}$ ) were observed in some experiments. This corresponds to in-plane domain sizes of 70–120  $\text{\AA}$  for the air-formed oxide (calculated via the Debye–Scherrer formula  $\Delta r = (0.9 \times 2\pi) / \text{fwhm} = 2.40/\sigma$ ). The transverse profile of all peaks is well described by a Gaussian with a width which is only slightly broader than in the radial direction. To describe the transverse profile, we utilize a profile which is generated from the radial profile convoluted with a sample dependent angular dispersion between  $0.9^\circ$  and  $1.2^\circ$ . Hence, the (111)-oriented planes of the air-formed NiO are perfectly parallel to those of the Ni substrate lattice. This was also found for much thicker oxide films formed by gas-phase oxidation at elevated temperature. In contrast, a much more complex behavior is observed for the passive film. In particular,  $\sigma_r$  and  $\sigma_t$  both depend strongly on the  $L$ -position of the diffraction peaks. For example, for  $\sigma_r$  average values of 0.042, 0.062, and  $0.110 \text{ \AA}^{-1}$  were obtained for the peaks at  $(0, a_{NiO}^*, c_{NiO}^*)$ ,  $(a_{NiO}^*, 0, 2c_{NiO}^*)$ , and  $(0, 0, 3c_{NiO}^*)$ , respectively. A similar  $L$  dependence was found for the transverse widths of these peaks as well as for the  $\sigma_r$  and  $\sigma_t$  of higher-order peaks. As will be shown in the following, this behavior can be rationalized by a slight tilt of the oxide lattice with respect to that of the Ni substrate.

The presence of a tilted oxide phase in the passive film on Ni(111) was first suggested by Maurice et al.,<sup>12,13</sup> based on ex situ STM observations of a highly stepped film morphology. From the average terrace width, they inferred a tilt of the NiO lattice with respect to the Ni substrate lattice by  $8 \pm 5^\circ$  along the [112] direction and attributed this to a favorable epitaxial lattice match of the oxide and the Ni lattice. In the diffraction pattern (see Figure 2b), a tilt by an angle  $\alpha$  would be directly manifested by a shift of the peak at  $(0, 0, 3c_{NiO}^*)$  from the specular axis as well as a shift of the peaks at  $(a_{NiO}^*, 0, 2c_{NiO}^*)$  to higher  $L$  and lower  $H$  and at  $(0, a_{NiO}^*, c_{NiO}^*)$  to lower  $L$  and lower  $K$  (and vice versa for  $-\alpha$ ). For the 3-fold lattice symmetry and the 2-fold tilt symmetry, six different domains should exist (Figure 2a, inset). Although all rotational domains exhibiting the same tilt direction should have the same probability due to symmetry reasons, no such symmetry exists for the two tilt

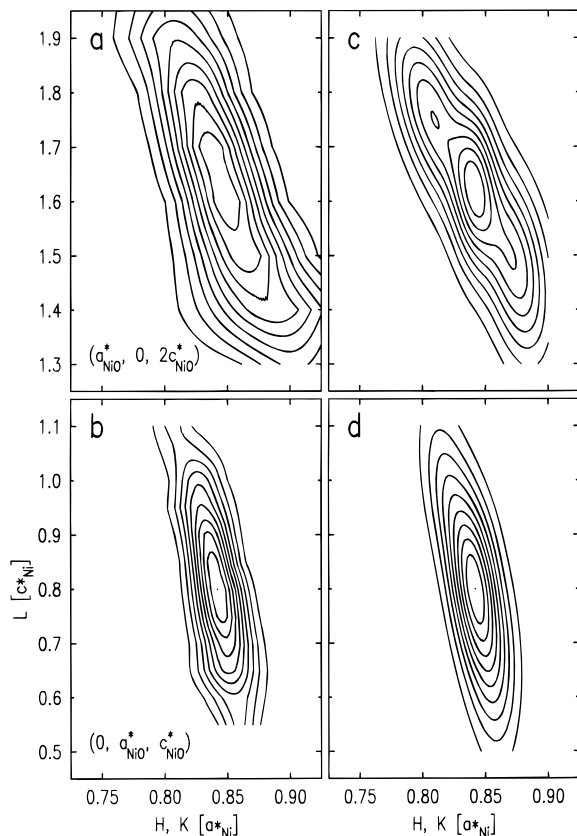


**Figure 4.** Contour plots showing (a,b) the peaks at  $(0, a_{\text{NiO}}^*, c_{\text{NiO}}^*)$  and  $(a_{\text{NiO}}^*, 0, 2c_{\text{NiO}}^*)$  for the passive film in 0.05 M  $\text{H}_2\text{SO}_4$  solution at 0.50 V (with background intensity subtracted) and (c,d) best fit results to a model where a continuous distribution of tilted phases was assumed.

directions. An extensive search around these positions for the passivated sample, however, gave no indication for peaks corresponding to a NiO phase with a well-defined lattice tilt of  $8^\circ$ . To clarify this point detailed mesh scans were performed around  $(0, a_{\text{NiO}}^*, c_{\text{NiO}}^*)$  and  $(a_{\text{NiO}}^*, 0, 2c_{\text{NiO}}^*)$ , which are shown in parts a and b of Figure 4. Although no distinct rotated peaks are visible in these scans, the peaks clearly are not described by simple elongated ellipsoids along  $L$  as expected for an untilted phase, but exhibit curved shapes characteristic for a lattice tilt. This behavior can be rationalized by a distribution of oxide phases with small, slightly different tilt angles. To quantify the tilt and tilt distribution, we model the tilt by the distribution function  $f(\alpha)$  and the intrinsic scattering from each domain as a three-dimensional Gaussian with widths  $\sigma_L$  and  $\sigma_H = \sigma_K$ . In the fitting procedure, the width, position, and amplitude of the distribution  $f(\alpha)$  could either be fixed or varied. Various forms of  $f(\alpha)$ , such as discrete  $\alpha$ , Gaussian, and error functions, and symmetric ( $f(\alpha) = f(-\alpha)$ ) as well as asymmetric ( $f(\alpha) \neq f(-\alpha)$ ) distributions were tried. Excellent fits (parts c and d of Figure 4) were obtained by modeling  $f(\alpha)$  as symmetric Gaussians with peak positions  $\alpha_0 = \pm 3.3^\circ$  and widths  $\sigma_a = 1.8^\circ$ . These results are in excellent agreement with recent in situ STM results by Zuili et al.,<sup>8</sup> which found a local tilt of the oxide ranging from  $0.7^\circ$  to  $3.4^\circ$  from the (111) axis. It is noteworthy that a tilted oxide phase with a similar broad distribution of tilt angles was also found in a study of Ni(100) gas-phase oxidation by LEED and STM,<sup>22</sup> indicating that such a wide distribution of tilt angles is not uncommon for these ultrathin oxide films.

In addition to the tilt distribution, the fitting provides oxide lattice parameters of  $a_{\text{NiO}}^* = (0.842 \pm 0.001)a_{\text{Ni}}^*$  and  $c_{\text{NiO}}^* =$

$(0.814 \pm 0.001)c_{\text{Ni}}^*$ . This corresponds to in-plane and surface normal lattice spacings of  $a_{\text{NiO}} = 2.959 \pm 0.004 \text{ \AA}$  and  $c_{\text{NiO}} = 7.50 \pm 0.01 \text{ \AA}$ , respectively. Hence, the in-plane lattice spacing of the passive film is (within the experimental error) identical to that of bulk NiO ( $a_{\text{NiO}} = 2.9549 \text{ \AA}$  at  $20^\circ \text{C}$ ), whereas in the air-formed oxide (see above) it is expanded by 1.1%. Along the surface normal direction, larger lattice expansions are found (relative to bulk NiO,  $c_{\text{NiO}} = 7.227 \text{ \AA}$ ) of 3.7% and 2.5% for the passive layer and the air-formed oxide film, respectively. A similar lattice expansion perpendicular to the surface for oxides on Ni(111) was observed by ex situ RHEED.<sup>9</sup> In addition, an average in-plane domain size of about  $80 \text{ \AA}$  and an oxide thickness of  $24 \text{ \AA}$ , i.e., considerably larger than for the air-formed oxide, can be calculated for the passive film from the model of the tilted oxide lattice. A similar thickness of the passive film was found in previous ellipsometric<sup>23,24</sup> and ex situ XPS studies.<sup>6,7</sup> The integrated NiO peak intensities of the passive film are in reasonable agreement with the NiO structure factors. A more detailed crystallographic analysis, which would give quantitative data on the passive oxide defect structure, is hampered by (i) the small size of the NiO unit cell, due to which only a limited number of peaks are accessible by the X-ray spectrometer, (ii) the very low intensities and consequently poor signal-to-background ratio of the higher-order Ni peaks, and (iii) the broad distribution of tilt angles, which contributes in a complex way to the peak widths.

The differences in the oxide film structure in air and in electrochemical environment have important consequences for the film stability and corrosion behavior. The coexistence of parallel and antiparallel domains for the oxide film in air implies the presence of noncoherent twin boundaries normal to the surface, which due to their rather open structure can provide paths of easy diffusion and hence play an important role in mass transport processes through the film.<sup>17</sup> In the passive film formed at the electrochemical interface, these twin boundaries are absent or at least significantly reduced in number, which, in addition to the larger thickness, may explain the higher stability against cathodic oxide reduction and the better corrosion resistance of the passive film as compared to the air-formed oxide.<sup>25</sup> The occurrence of different tilt angles for the passive film only results in small-angle boundaries between the oxide grains, which still allow a dense packing at the grain boundary, and therefore should not significantly affect the transport processes through the film. Finally, the reversion of the passive film into a mixed parallel/antiparallel oxide upon emersion from the electrolyte may have implications for the atmospheric corrosion of Ni. Although the mechanism of this process is not completely understood, it is clear that this will result in the creation of new defects, such as twin boundaries, which may exhibit an enhanced reactivity for corrosion reactions after reimmersion into electrolyte. This would cause an increased corrosion rate in dry-wet cycles, i.e., under conditions common in outdoor atmospheric corrosion.

#### 4. Summary

In summary, these results show that although the oxide films on Ni(111) always consist of an aligned, (111)-oriented NiO phase, distinct differences exist between the oxide formed in the gas phase and the passive film present at the metal-electrolyte interface. Beside the different thickness, two major, qualitative differences concerning the orientation of the oxide with respect to the Ni substrate lattice were found. In contrast to the air-formed oxide, the lattice of the passive film exhibits (i) a well-defined antiparallel orientation and (ii) a slight tilt relative to the substrate lattice with a broad distribution of tilt

angles coexisting on the surface. The latter is a direct confirmation of the model proposed by Maurice et al.<sup>12,13</sup> on the basis of their ex situ STM observations. These differences may contribute to the different stability of these oxide films, e.g., with respect to electrochemical reduction and corrosion resistance.

**Acknowledgment.** We gratefully acknowledge financial support and a fellowship for O.M.M. by the Deutsche Forschungsgemeinschaft. Brookhaven National Laboratory is supported by the Department of Energy under Contract DE-AC-02-98CH10886. Also, we thank P. Woodward for the use of his tube furnace and J. Wang and P. Marcus for helpful discussions.

### References and Notes

- (1) Sato, N.; Okamoto, G. In *Electrochemical Materials Science*; Bockris, J. O., Conway, B. E., Yeager, E., White, R. E., Eds.; Plenum Press: New York, 1981; pp 193–245.
- (2) MacDougall, B.; Graham, M. J. In *Corrosion Mechanisms in Theory and Practice*; Marcus, P., Oudar, J., Eds.; Dekker: New York, 1995; pp 143–174.
- (3) Wiesler, D. G.; Toney, M. F.; Melroy, O. R.; McMillan, C. S.; Smyrl, W. H. *Surf. Sci.* **1994**, *302*, 341–349.
- (4) Toney, M. F.; Davenport, A. J.; Oblonsky, L. J.; Ryan, M. P.; Vitus, C. M. *Phys. Rev. Lett.* **1997**, *79*, 4282–4285.
- (5) Toney, M. F.; Ryan, M. P.; Oblonsky, L. J.; Davenport, A. J. *Synchrotron Radiat. News* **1998**, *11*, 5–11.
- (6) Marcus, P.; Oudar, J.; Olefjord, I. *J. Microsc. Spectrosc. Electron.* **1979**, *4*, 63–72.
- (7) Hoppe, H.-W.; Strehlow, H.-H. *Surf. Interface Anal.* **1989**, *14*, 121–131.
- (8) Zuili, D.; Maurice, V.; Marcus, P. *J. Electrochem. Soc. Proc.* **1997**, *97-26*, 1013–1024.
- (9) MacDougall, B.; Cohen, M. *J. Electrochem. Soc.* **1974**, *121*, 1152–1159.
- (10) MacDougall, B.; Cohen, M. *J. Electrochem. Soc.* **1976**, *123*, 191–197.
- (11) Oudar, J.; Marcus, P. *Appl. Surf. Sci.* **1979**, *3*, 48–67.
- (12) Maurice, V.; Talah, H.; Marcus, P. *Surf. Sci.* **1993**, *284*, L431–L436.
- (13) Maurice, V.; Talah, H.; Marcus, P. *Surf. Sci.* **1994**, *304*, 98–108.
- (14) Suzuki, T.; Yamada, T.; Itaya, K. *J. Phys. Chem.* **1996**, *100*, 8954–8961.
- (15) Wang, J.; Ocko, B. M.; Davenport, A. J.; Isaacs, H. S. *Phys. Rev. B* **1992**, *46*, 10321–10338.
- (16) Lawless, K. R.; Young, F. W.; Gwathmey, A. T. *J. Chim. Phys.* **1956**, *53*, 667–674.
- (17) Cathcart, J. V.; Petersen, G. F.; Sparks, C. J. *J. Electrochem. Soc.* **1969**, *116*, 664–668.
- (18) Graham, M. J.; Hussey, R. J.; Cohen, M. *J. Electrochem. Soc.* **1973**, *120*, 1523–1529.
- (19) Scherer, J.; Magnussen, O. M.; Ocko, B. M.; Behm, R. J. Unpublished.
- (20) Siejka, J.; Cherki, C.; Yahalom, J. *J. Electrochem. Soc.* **1972**, *119*, 991–998.
- (21) MacDougall, B.; Mitchell, D. F.; Graham, M. J. *J. Electrochem. Soc.* **1985**, *132*, 2895–2898.
- (22) Bäumer, M.; Cappus, D.; Kühlenbeck, H.; Freund, H.-J.; Wilhelmi, G.; Brodde, A.; Neddermeyer, H. *Surf. Sci.* **1991**, *253*, 116–128.
- (23) Kang, Y.; Paik, W. *Surf. Sci.* **1987**, *182*, 257–268.
- (24) Ohtsuka, T.; Schoner, K.; Heusler, K. E. *J. Electroanal. Chem.* **1978**, *93*, 171–182.
- (25) MacDougall, B.; Mitchell, D. F.; Graham, M. J. *Isr. J. Chem.* **1979**, *18*, 125–130.